Textures and Microstructures, Vol. 33, pp. 303–319
Reprints available directly from the publisher
Photocopying permitted by license only

EQUILIBRIUM OF ELASTIC MICROSTRESSES IN TEXTURED METAL MATERIALS

YU. PERLOVICH[a], H.J. BUNGE[b,*], M. ISAENKOVA[a] and V. FESENKO[a]

[a]*Moscow Engineering Physics Institute, Kashirskoe shosse 31, 115409 Moscow, Russia;* [b]*Department of Physical Metallurgy TU Clausthal, 38678 Clausthal-Zellerfeld, Germany*

(Received 10 July 1998)

In order to study the distribution of lattice elastic microstresses in textured metal materials, pole figures of X-ray line peak position were constructed on the basis of data, obtained by diffractometric texture measurements using a position sensitive detector. The data treatment involves recalculation of the Bragg angle $2\theta_{\varphi\psi}$ into the relative deviation of the interplanar spacing from the weighted average level $\Delta d/d_{av}$. Depending on the texture character, different modes of microstress equilibrium take place. A common feature of most lattice deformation pole figures is the cross-wise pattern, consisting in alternation of quadrants with predominance of lattice elastic extension and compression. In cases of simple rolling textures, the microstress equilibrium is attained by some additional ways, among which there are breaking of texture maxima into halves with opposite signs of elastic deformation, predominance of one-sign elastic deformation within different texture maxima, development of stretched zones with opposite signs of elastic deformation at slopes of texture maxima. In some cases the identical microstress distribution in all quadrants of pole figure is observed.

Keywords: Rolling texture; Peak position pole figure; Lattice elastic deformation; Microstress equilibrium

1. INTRODUCTION

The recent development of X-ray texture diffractometry resulted in elaboration of the new methods to study the substructure inhomogeneity

* Corresponding author.

and the distribution of elastic microstresses in textured metal materials. These methods consist in measurement and construction of pole figures for X-ray line broadening and peak position (WPF and PPF, respectively), which, along with usual pole figures, i.e. pole figures for X-ray line integral intensity (IPF), give a full description of the studied object in terms of diffraction parameters (Perlovich *et al.*, 1996; 1997). Since parameters of the registered X-ray line (hkl) characterize the condition of the crystalline lattice in grains of the studied textured sample along the normal to the reflecting planes $\{hkl\}$, WPF$\{hkl\}$and PPF$\{hkl\}$ represent the distribution of this condition in the orientational space. While the line broadening is connected with the coherent domain size and the lattice distortion, the peak position depends on the value and the sign of elastic stresses acting along the corresponding normal $\langle hkl \rangle$ (Taylor, 1961).

Previously there were some attempts already to construct both WPF and PPF. Evstyuchin and Perlovich (1973) and Perlovich (1983, 1994) constructed WPF's for cold-rolled molybdenum and revealed the following correlation between the distributions of integral intensity and half-width of X-ray lines, i.e. between IPF and WPF: as the orientation of reflecting grains moves from the texture maximum towards the texture minimum, the half-width of the registered X-ray line increases gradually, varying over a very wide range. The proposed model explains an increase of lattice distortion and domain dispersion at the periphery of texture maxima by operation of the mechanism responsible for maintenance of the stable orientations depending on features of the Schmid factor distribution. The similar effect was observed later by Barral *et al.* (1986, 1987) for cold-rolled low-carbon steel by use of the synchrotron radiation.

As for PPF construction, a large series of works on this theme was carried out mostly in the Karlsruhe University. Hoffmann *et al.* (1983, 1984, 1986) presented distributions of lattice deformation in cold-rolled ARMCO-iron and structural steel, obtained by use of a modified ψ-diffractometer and a position sensitive detector (PSD). However, as it was clearly stated by Maurer *et al.* (1987), the main aim of their studies was to elaborate a procedure, which would remove effects of the inhomogeneous microstress distribution (kind II) and allow to determine reliably residual macrostresses (kind I) by the $\sin^2\psi$-method. Therefore, they neither indicated characteristic features of the microstress

distribution in rolled materials nor revealed principles, which control this distribution. Nevertheless, some obvious features of lattice deformation pole figures, presented in the above-cited works, agree with data of our paper, based on the analysis of numerous PPFs for various rolled materials.

The present condition of the X-ray diffractometric technique is characterized by further perfection both of hardware and software. When using automated texture diffractometers of a new generation with PSD and the complex of programs for computer treatment of obtained experimental data (Wcislak and Bunge, 1996), the measurement of WPF and PPF becomes a routine procedure, incomparable by its capacities with earlier ones. These capacities were used in the given work, whose aim was to systematize observed PPFs, i.e. distributions of lattice elastic deformation in several studied metal materials.

2. EXPERIMENTAL PROCEDURE AND DATA TREATMENT

Measurements of all presented pole figures were carried out by use of the X-ray texture diffractometer SIEMENS D500/TX equipped with a PSD and a multichannel analyser. The simultaneous viewing angle of the PSD was 9°, whereas the angular resolving power was chosen 0.05°. This way, by using Cu K_α radiation, a diffraction spectrum was obtained for each orientation of studied samples. Incomplete pole figures with an angular radius of 70° were measured. By step-wise rotation of the sample in steps $\Delta\varphi$ and $\Delta\psi$ of 5° or 2.5°, the total number of measurement points in the pole figure was respectively 1009 or 2017.

The subsequent computer treatment of the obtained data used a fitting procedure, consisting in the search of such X-ray line parameters, which provide a minimal difference between experimental results and their approximation, i.e. minimal fitting error (Wcislak *et al.*, 1993). The following parameters of the X-ray line were varied with the aim to minimize the fitting error: maximal intensity, half-width, peak position, proportion of Gauss and Cauchy functions in the approximating pseudo-Voigt function. The doublet structure of the K_α-line was taken into account. Since our interest is in the physical line profile function, it was necessary to separate it from the instrumental profile function, with

which, by means of convolution, it forms the experimentally measured profile (Taylor, 1961). In order to obtain the instrumental function as well as the defocalization effect depending on the tilt angle ψ, similar measurements were carried out with a textureless annealed standard. In more detail the used procedure of data treatment is described by Perlovich *et al.* (1997). Here it should be underlined that calculation of the peak position on the basis of PSD data as well as construction of PPF require to fulfil the whole cycle of data treatment, necessarily including calculation of all parameters of the registered X-ray line for each position (φ, ψ) of the sample. By doing so, the corresponding pole figures of different types, that is IPF, WPF and PPF, are constructed in parallel to one another.

We laid in the basis of the PPF analysis the natural principle of the equilibrium of elastic stresses. By definition, elastic stresses of second kind, i.e. microstresses, are equilibrated within a volume of several neighboring grains. The volume irradiated in the course of X-ray texture diffractometric measurement in most cases is sufficiently large to satisfy the conditions for microstress equilibrium. Therefore, the texture pole figure is formed by reflections from regions (grains, subgrains, blocks, and the like), whose crystalline lattice experiences alternatively elastic deformations of opposite signs relative to some average level corresponding to the local value of elastic stresses of first kind, i.e. macrostresses. Microstresses associated with these elastic deformations are known to be mutually balanced within the reflecting volume.

However, the preceding refers only to lattice deformations taken independently along normals of interest, as if our sample consists of needle-wise structure elements. For the sake of the stress equilibrium analysis such a view is worthwhile and acceptable. But in reality, each grain has several normals of the same type, so that lattice elastic deformations along these normals are interconnected and require the tensor description. In principle, the used approach for the first time allows to determine components of the deformation tensor for different grain groups within the textured polycrystal.

In order to reveal systematic features in the peak position distribution, values of the Bragg angle $2\theta_{\varphi\psi}$ in some cases were converted into values $\Delta d/d_{\mathrm{av}}$, that is the relative deviation of the interplanar spacing $d_{\varphi\psi}$ from the weighted average level d_{av}. This level is determined

as follows:

$$d_{av} = \sum_{\varphi,\psi} s_\psi I_{\varphi,\psi} d_{\varphi,\psi} \Big/ \sum_{\varphi,\psi} s_\psi I_{\varphi,\psi}, \tag{1}$$

where s_ψ is the area fraction of the stereographic projection, falling on each point by the tilt angle ψ, and $I_{\varphi\psi}$ is the peak intensity for the point (φ, ψ). In consequence of the conversion, PPFs experience some changes, connected with a conventional assumption that in points with zero intensity the value $\Delta d/d_{av}$ is equal to zero also. As a result, regions with opposite signs of $\Delta d/d_{av}$ prove to be visually separated.

Since calculation of d_{av} is carried out by the incomplete pole figure, some error is inevitable, except some special cases. The error depends on texture features of the sample and decreases with decreasing fraction of normals within the invisible part of IPF as well as owing to the mutual balance of elastic microstresses directed along these normals. At the same time, the symmetric character of all obtained PPF testifies that usually the error by d_{av} calculation does not influence the $\Delta d/d_{av}$ distribution in the limits of the obtained part of the pole figure.

In the present paper data are given for the following materials:

- single crystals of the Ti–Ni shape memory alloy (Ti–48%Ni–2%Fe), rolled in the phase B2 (BCC lattice ordered by the CsCl type) with various initial orientations up to different deformation degrees;
- the alloy Zr–20%Nb both in rolled and annealed conditions, consisting of the BCC phase β and/or the HCP phases α or ω;
- cold-rolled foils of Nb (BCC lattice);
- cold-rolled plate of pure Ti (HCP lattice).

Typical distributions of the lattice elastic deformation are shown in order to demonstrate the ways, which "are chosen" by studied materials to attain the equilibrium of elastic microstresses.

3. RESULTS: OBSERVED MODES OF MICROSTRESS EQUILIBRIUM

A common feature of most of the presented PPFs is the cross-wise pattern consisting in alternation of quadrants with opposite predominant signs of lattice elastic deformation. This is an experimental fact, which seems to

be unpredictable on the basis of mental models. First, when the texture of the rolled sample is simple, the distribution of lattice elastic deformation manifests some additional features worthy of special attention. These features are highlighted in the titles of the following paragraphs as distinguishing characteristics of different equilibrium modes.

A direct manifestation of the inhomogeneous distribution of lattice elastic deformation, which is evident even before the data treatment, consists in the gradual shift of the registered X-ray line, as we go

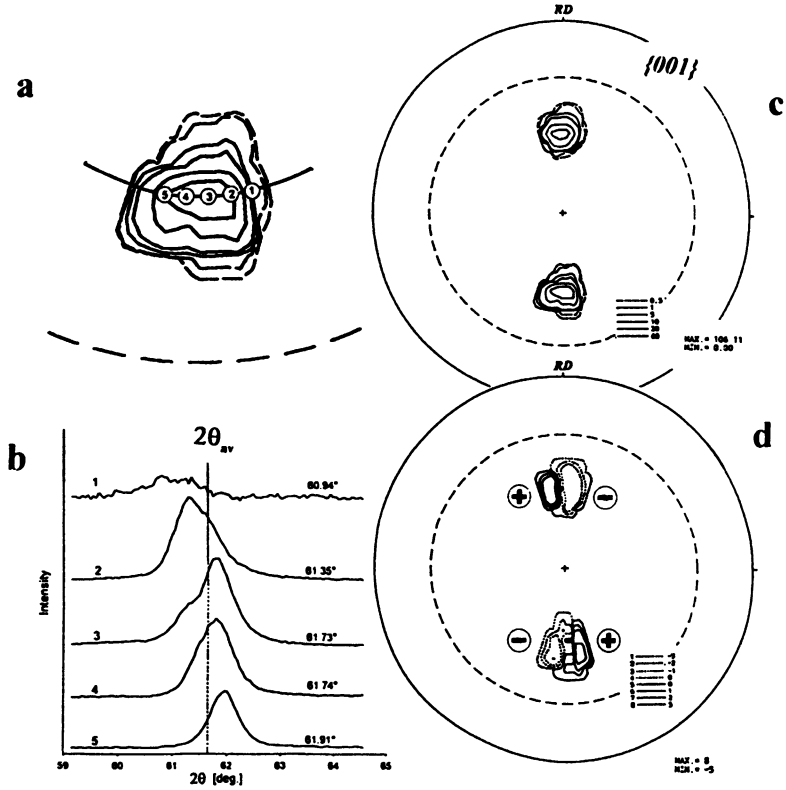

FIGURE 1 The distribution of lattice elastic deformation along crystallographic normals ⟨001⟩ in the rolled Ti–Ni single crystal with a one-component texture. Initial orientation – {011}⟨011⟩, $\varepsilon = 10\%$. (a) Arrangement of successive points of measurement within the lower texture maximum in IPF{001}(c); (b) X-ray lines (002) registered in the respective points of (a); (c) IPF {001} obtained by use of the X-ray line (002); (d) PPF {001} constructed in units of $(\Delta d/d) \times 10^3$; regions of elastic extension and compression are shown with signs "+" and "−", respectively.

point-by-point through a texture maximum at a fixed tilt angle ψ, so that the same instrumental broadening takes place. As an example, Fig. 1 shows a number of experimental X-ray lines (002), measured at successive points within the lower texture maximum in IPF{001} for the Ti–Ni single crystal, which had been rolled by $\varepsilon = 10\%$ in the stable initial orientation $\{011\}\langle 011\rangle$. The shown profiles of the X-ray line did not experience as yet any treatment, but their relative positions agree with the indicated nearby values of the Bragg angle $2\theta_{002}$ obtained later by approximation and taking into account instrumental effects. A vertical line marks the weighted average value of the Bragg angle, calculated for the whole pole figure.

It can be seen that in the center of the texture maximum the X-ray line is composed of two lines spaced apart. Sometimes this effect is more well-defined, so that there arises a distinct impression of two phases to be present in the studied sample. Such a situation is illustrated by Fig. 2, where, for the same rolled single crystal ($\varepsilon = 10\%$) with the initial orientation $\{011\}\langle 011\rangle$, the X-ray lines (011) are shown, corresponding to the section of the lower left maximum in IPF{011}. Here the points of successive X-ray line measurements are positioned along the boundary between regions with opposite signs of elastic microstresses. As a result, both regions occur simultaneously within the PSD range of vision. Besides, an important conclusion can be made on the basis of these latter observations: both the lattice deformation and elastic microstresses change discretely, i.e. stepwise, in the orientational space, so that an obviously continuous distribution is the result of overlap together with limited angular resolution.

3.1 One-Component Texture: Breaking of Texture Maxima into Halves with Opposite Signs of Elastic Deformation

Rolled Ti–Ni single crystals with a one-component rolling texture manifest the most spectacular mode of microstress equilibrium, which consists in a division of the texture maxima into two halves, characterized alternatively by opposite signs of elastic deformation, i.e. by elastic extension ("+") or compression ("−"). As a typical example, Figs. 1 and 2 show IPF (c) as well as PPF (d), obtained by X-ray lines (002) and (011), respectively, for the Ti–Ni single crystal rolled by $\varepsilon = 10\%$ in the stable initial orientation $\{011\}\langle 011\rangle$. Both IPFs consist of isolated texture

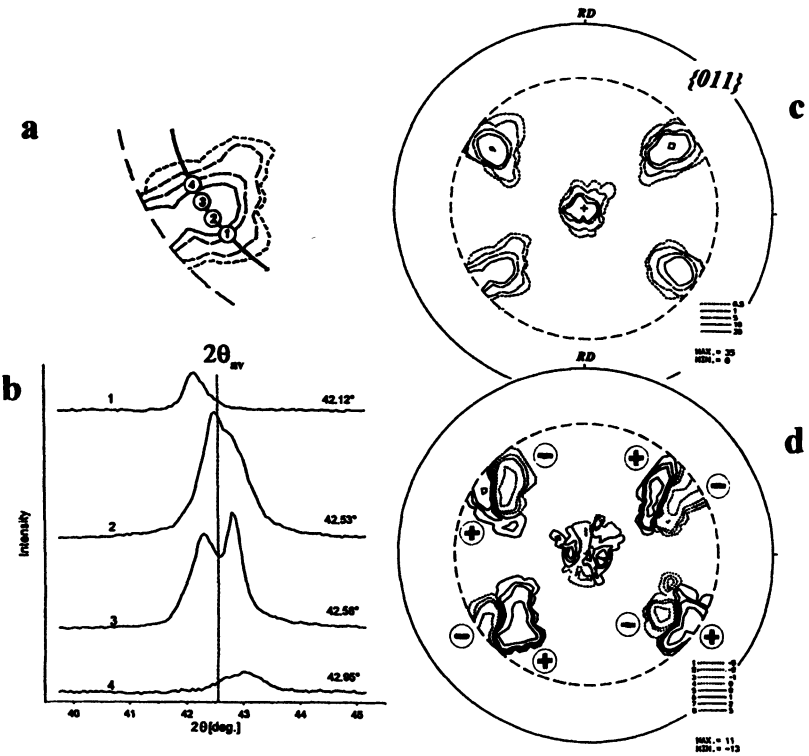

FIGURE 2 The distribution of lattice elastic deformation along crystallographic normals ⟨011⟩ in the rolled Ti–Ni single crystal with a one-component texture. Initial orientation – {011}⟨011⟩, $\varepsilon = 10\%$. (a) Arrangement of successive points of measurement within the lower left texture maximum in IPF{011}(c); (b) X-ray lines (011) registered in the respective points of (a); (c) IPF {011} obtained by use of the X-ray line (011); (d) PPF {011} constructed in units of $(\Delta d/d) \times 10^3$; regions of elastic extension and compression are shown with signs "+" and "−", respectively.

maxima, whose positions correspond to projections of normals ⟨001⟩ and ⟨011⟩ for the initial orientation of the single crystal. In both PPF all these maxima prove to be divided into approximately equal regions of elastic extension and compression in such a manner that they are mutually equilibrated about diameters RD–RD and TD–TD.

As for the distribution of elastic deformation along cubic axes (Fig. 1(d)), its obvious principle is the following: whilst one normal ⟨001⟩ of some crystalline block is placed within the region of extension, belonging to the upper texture maximum, another one of its normals

⟨001⟩ is in the region of compression, belonging to the lower maximum. At the same time, the elastic deformation of a neighboring block, with an orientation close to the first one, can be reversed, i.e. compression along the normal in the upper texture maximum and extension along the normal in the lower maximum. Owing to such distribution of elastic deformation, the total mutual equilibrium of substructure elements in the rolled single crystal becomes possible. It is significant that blocks with the same character of elastic deformation form a compact region in the orientational space, separated distinctly from the region of the reverse deformation character.

3.2 Two-Component Texture: Predominance of One-Sign Elastic Deformation within Different Texture Maxima

When the texture of the rolled single crystal is formed by a pair of mutually equivalent components, these components equilibrate one another owing to the predominant alternative action of extensive and compressive elastic stresses within the respective texture maxima. Figures 3 and 4 demonstrate such a situation by the example of a Ti–Ni single crystal rolled in the initial orientation {001}⟨011⟩ by the deformation degree of 58%. The rolling texture of the sample consists of two final stable components {111}⟨011⟩, having three maxima each in the IPF {001} (Fig. 3). Maxima of these two components are labelled A and B, whereas three signs (circle, square and romb) are used to distinguish different maxima of the same set. The correlation diagrams "peak position – integral intensity" in Fig. 4(a) and (b) visualize the difference between texture maxima of both sets (A and B) in IPF {001} as for lattice deformation along directions corresponding to the measurement points within these maxima. Really, circles and squares are situated predominantly in different regions of the diagrams, what is especially true for the component A. While in Fig. 4(a) circles are arranged in the lower region of the diagram, in Fig. 4(b) they concentrate in the upper region, providing the equilibrium of elastic microstresses, which are localized in different texture components.

Thus, unlike the above-considered case of a one-component texture, the majority of substructure elements corresponding to each component in the case of a two-component texture are deformed elastically in a similar manner, i.e. in the limits of any texture maximum either extension

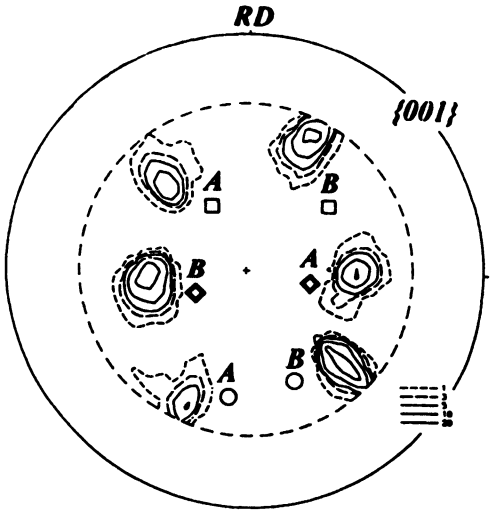

FIGURE 3 IPF{001} for the rolled Ti–Ni single crystal with a two-component texture. Initial orientation – $\{001\}\langle 011\rangle$, $\varepsilon = 58\%$. The used symbols are only labels for different texture maxima of the components A and B, but do not indicate their "ideal" positions.

or compression takes place predominantly. Exceptions are texture maxima situated at the diameter TD–TD, where elastic microstresses, both extensive and compressive, are close to the average level.

Since mutually equilibrated elastic microstresses of opposite signs are located in different texture components, it follows that crystalline blocks corresponding to these components are mixed in the studied volume and each block of the first component has blocks of the second component among its nearest neighbors.

3.3 Sharp Polycomponent Texture with Features of Axiality: Stretched Zones with Opposite Signs of Elastic Microstresses at Slopes of Texture Maxima

Textures of this type are most usual for cold-rolled polycrystalline metal materials. The axiality of these textures consists in the stretching of their maxima in pole figures along parallels of the stereographic projection, i.e. the developed rolling texture includes a continuous succession of components with the common RD. Elastic microstresses, in this case, are

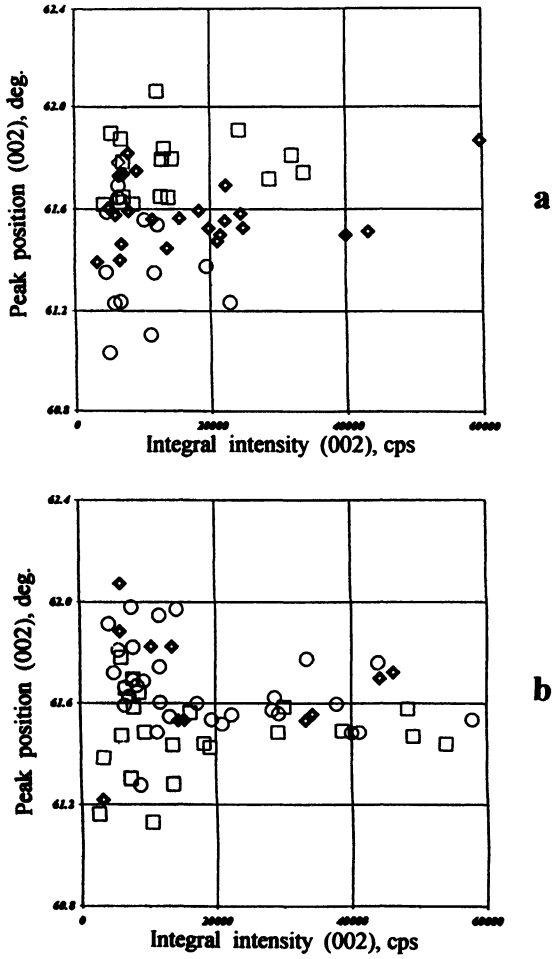

FIGURE 4 Correlation diagrams "peak position – integral intensity" for the rolled Ti–Ni single crystal with a two-component texture (initial orientation – {001}⟨011⟩, $\varepsilon = 58\%$). The used X-ray line – (002). Diagrams for points within texture maxima of the components A and B in IPF{001} (Fig. 3) are shown in (a) and (b), respectively. The used symbols are labels of different texture maxima in IPF{001}.

distributed in such a manner that zones of extension and compression are aligned parallel with texture maxima at their opposite slopes. When the long narrow texture maximum is located at the center of IPF along its diameter TD–TD, zones of elastic extension and compression form a

cross-wise pattern, so that both diameters of pole figure separate zones with opposite signs of elastic deformation.

These features are demonstrated for the alloy Zr–20%Nb, which was quenched from the β-region of the phase diagram and then rolled up to high deformation degrees. In the rolled state it consists only of β-Zr, so that its rolling texture is typical for materials with the BCC crystalline lattice. Owing to the high deformation degree, IPF{011} in Fig. 5(a) shows a significant axiality. The corresponding distribution of the Bragg angle 2θ in Fig. 5(b) distinctly manifests, that cross-hatched zones of increased 2θ values are shifted relative to the texture maxima to their slopes and that the distributions within first and third as well as second and fourth quadrants are similar.

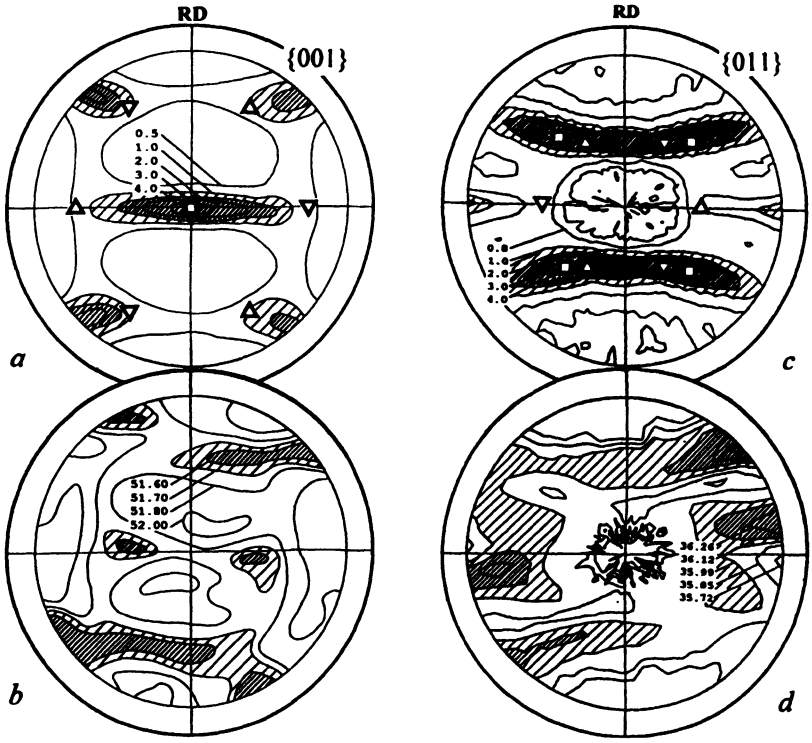

FIGURE 5 The distribution of lattice elastic deformation along crystallographic normals ⟨001⟩ and ⟨011⟩ in the β-phase of the quenched rolled alloy Zr–20%Nb: IPF{001} (a) and PPF(002) (b) obtained by use of the X-ray line (002); IPF {011} (c) and PPF(011) (d) obtained by use of the X-ray line (011). Both PPFs are constructed in units of 2θ. □ – {001}⟨011⟩; △,▽ – {111}⟨011⟩.

The same situation is seen in pole figures for the ω-Zr phase, obtained in the quenched rolled sample of the same alloy by annealing at 400°C (Fig. 6). The distribution of basal normals was analyzed by use of the X-ray line $(0001)_\omega$. The texture of the ω-phase was formed by the phase transformation $\beta \rightarrow \omega$ characterized by the arrangement of the planes $(0001)_\omega$ parallel to the planes $\{111\}_\beta$ (Douglass, 1971). PPF$(0001)_\omega$ in Fig. 6 testifies that the derivative ω-phase inherits the mode of elastic stress distribution formed in the original β-phase by rolling. According to the estimation, some local increase of the lattice elastic deformation takes place by the phase transformation $\beta \rightarrow \omega$: the total area of regions, where $|\Delta d/d| > 0.2$, becomes larger. Since both the HCP ω-phase and the BCC β-phase show the same cross-wise pattern of elastic stress distribution, it is evident that this pattern does not depend on the lattice symmetry or the number of equivalent normals (in the case of the ω-phase only one normal $\langle 0001 \rangle$ corresponds to each grain within the pole figure), but is determined by factors of the other level.

3.4 Texture with Large Regions of Scattering: Alternation of Quadrants with Opposite Signs of Elastic Deformation

This is the most general case. As the area of IPF, where intensity values exceed the background level, increases, the PPF character loses its

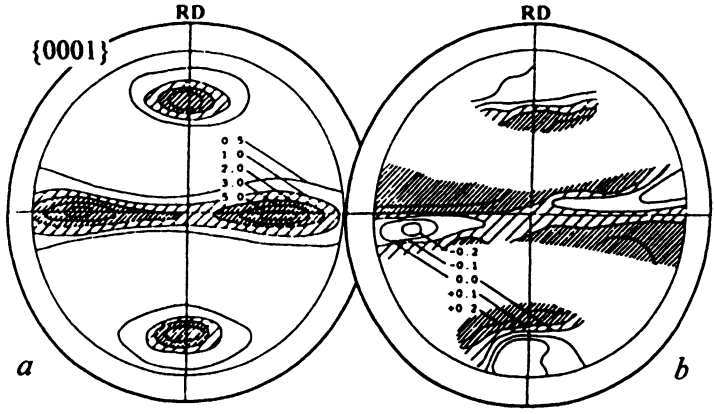

FIGURE 6 The distribution of lattice elastic deformation along crystallographic normals $\langle 0001 \rangle$ in the ω-phase of the quenched rolled alloy Zr–20%Nb after its annealing at 400°C. (a) IPF(0001) obtained by use of the X-ray line (0002); (b) PPF(0001) constructed in units of $\Delta d/d \times 10^2$.

clearness and becomes more complicated. Sometimes such an effect is connected with the coexistence of texture components, formed at successive stages of rolling due to the operation of different micromechanisms of plastic deformation. However, even in those cases, when the distribution of lattice elastic deformation seems to be rather random, a predominance of extensive or compressive stresses remains often evident within alternating quadrants of PPF.

In Fig. 7 IPF and PPF are presented for a foil of Nb, whose rolling texture contains components of different types and shows a significant scattering formed by disperse crystallites with intermediate orientations. Along with the components $\{001-113-112\}\langle 011\rangle$, which are usual for the rolling texture of BCC metals, the component $\{011\}\langle 001\rangle$ is present

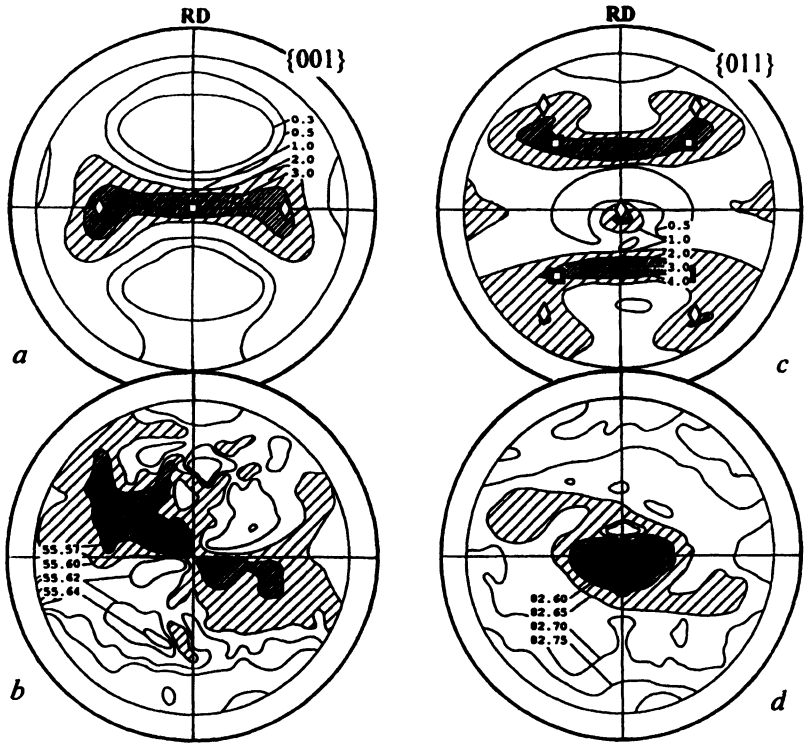

FIGURE 7 The distribution of lattice elastic deformation in the cold-rolled foil of Nb. IPF{001} (a) and PPF(002) (b) obtained by use of the X-ray line (002); IPF{011} (c) and PPF(022) (d) obtained by use of the X-ray line (022). Both PPFs are constructed in units of 2θ. □ – $\{001\}\langle 011\rangle$, ◇ – $\{011\}\langle 001\rangle$.

in the texture of the studied foil. Some additional mechanism of plastic deformation is supposed to be responsible for development of the latter component, so that its substructure features differ from those of the main set (Perlovich *et al.*, 1997). Besides that, maxima of different components are almost overlapping in the IPF of both types, i.e. {001} and {011}. As a result, the given distributions of normals are essentially more complicated than those presented above in Section 3.3. Correspondingly, the distribution of elastic deformation loses its regular character. Nevertheless, it retains the cross-wise pattern, i.e. quadrants showing predominant extension alternate in the PPF with quadrants showing predominant compression.

3.5 Identical Distribution of Lattice Elastic Deformation within *All* Quadrants

However, in some cases the distribution of lattice elastic deformation, obtained for rolled materials, proves to be symmetric about both diameters RD and TD, being identical within all four quadrants of PPF. As compared with the above-considered cross-wise pattern, this mode of stress equilibrium seems to be more simple, since it does not require additional ordering of microstresses depending on their sign in

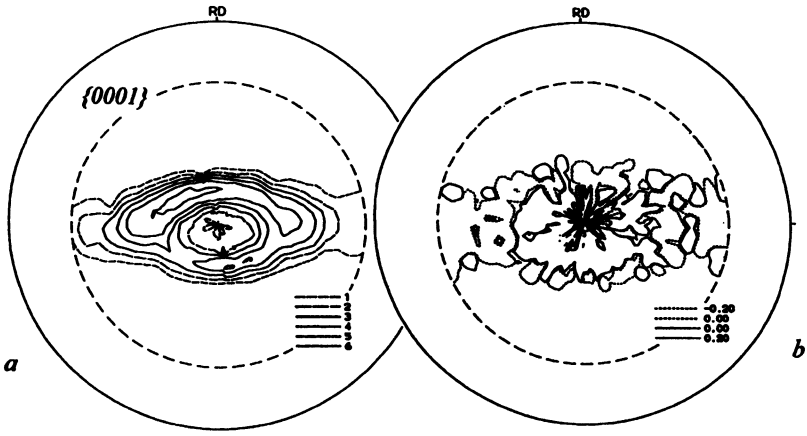

FIGURE 8 The distribution of lattice elastic deformation along crystallographic normals ⟨0001⟩ in the α-phase of the cold-rolled plate of pure Ti. (a) IPF(0001) obtained by use of the X-ray line (0004); (b) PPF(0001) constructed in units of $\Delta d/d \times 10^2$.

alternating quadrants. Nevertheless, the symmetric distribution of lattice elastic deformation is observed much more seldom than the cross-wise one.

In particular, a distribution of this type developed in a plate of pure Ti by cold rolling, as it is seen in Fig. 8. In the studied sample the final rolling texture did not form yet, so that it contains grains, in which various micromechanisms of plastic deformation are operating – basal, prismatic and pyramidal slip, twinning as well as their combinations (Vishnyakov *et al.*, 1979). Owing to such variety of mechanisms, grains differ significantly in their substructure features according to the position of the basal normal in IPF. As a result, equilibrium of elastic stresses may be obtained within each quadrant of PPF.

SUMMARY

1. The distribution of lattice elastic deformation as well as the mode of elastic microstress equilibrium in rolled-metal materials depend on the character of the rolling texture.
2. For the majority of studied materials the most common feature of the distribution is a cross-wise pattern, consisting in alternation of quadrants with predominance of elastic extension and compression.
3. For simple textures the following modes of microstress equilibrium were revealed: breaking of texture maxima into halves with opposite signs of elastic deformation, predominance of one-sign elastic deformation within different texture maxima, development of stretched zones with opposite signs of elastic microstresses at slopes of texture maxima.
4. The principal character of the microstress distribution can be inherited by phase transformation.
5. Besides the cross-wise pattern of microstress equilibrium, in some cases the identical microstress distribution in all quadrants of pole figure takes place.

Acknowledgement

The authors gratefully acknowledge sponsoring of this work by the German Research Foundation (DFG).

References

Barral, M., Lebrun, J.L., Sprauel, J.M. and Maeder, G. (1987). X-ray stress analysis of textured materials. Calculations of X-ray compliances with the ODF. In: *Theoretical Methods of Texture Analysis*. Ed. by H.J. Bunge. Deutsche Gesellschaft für Metallkunde, Informationsgesellschaft Verlag, pp. 355–364.

Barral, M., Sprauel, J.M., Lebrun, J.L. and Maeder, G. (1986). X-ray macrostress determination and microstrain evaluation on a textured material. In: *Experimental Techniques of Texture Analysis*. Ed. by H.J. Bunge. Deutsche Gesellschaft für Metallkunde, Informationsgesellschaft Verlag, pp. 419–428.

Douglass, D.L. (1971). "The Metallurgy of Zirconium". International Atomic Energy Agency, Vienna, 465 p.

Evstyuchin, A.I. and Perlovich, Yu. (1973). X-ray method for the selective investigation of grains with given crystallographic orientations as applied to rolled materials. In: *Metallurgy and Metal Science of Pure Metals*. Atomizdat, Moscow, pp. 32–38 (in Russian).

Hoffmann, J., Maurer, G., Neff, H. and Macherauch, E. (1986). A PSD-diffractometer for the determination of texture and lattice deformation pole figures. In: *Experimental Techniques of Texture Analysis*. Ed. by H.J. Bunge. Deutsche Gesellschaft für Metallkunde, Informationsgesellschaft Verlag, pp. 409–418.

Hoffmann, J., Neff, H., Scholtes, B. and Macherauch, E. (1983). *Härterei – Tech. Mitt.*, **38**, 180–183.

Hoffmann, J., Neff, H., Scholtes, B. and Macherauch, E. (1984). Texture pole figures and lattice deformation pole figures of materials having pronounced deformation textures. In: *Proceedings of the 5th Risoe International Symposium on Metallurgy and Material Science*, Risoe National Laboratory, Roskilde, Denmark, pp. 595–600.

Maurer, G., Neff, H., Scholtes, B. and Macherauch, E. (1987). Textur- und Gittereigendeformationszustände kaltgewalzter unlegierter Stähle. *Z. Metallkunde*, **78**, 1–7.

Perlovich, Yu. (1983). Inhomogeneity of strain hardening, recovery and recrystallization in alloyed molybdenum with the developed crystallographic texture. In: *Structure, Texture and Mechanical Properties of Deformed Molybdenum Alloys*. Ed. By V.I. Trefilov, Naukova Dumka, Kiev, pp. 87–145 (in Russian).

Perlovich, Yu. (1994). Development of strain hardening inhomogeneity during texture formation under rolling of BCC-metals. In: *Numerical Prediction of Deformation Processes and the Behaviour of Real Materials*. Proceeding of the 15th Risoe International Symposium on Materials Science. Ed. by S.I. Andersen *et al.*, Risoe National Laboratory, Roskilde, Denmark, pp. 445–450.

Perlovich, Yu., Bunge, H.J., Fesenko, V. and Isaenkova, M. (1996). X-ray study of structure inhomogeneity in textured materials. In: *Textures of Materials*. Proceedings of ICOTOM-11. Ed. by Liang Zhide *et al.*, International Academic Publishers, Beijing, China, pp. 1455–1460.

Perlovich, Yu., Bunge, H.J. and Isaenkova, M. (1997). Inhomogeneous distribution of residual deformation effects in textured BCC metals. *Textures and Microstructures*, **29**, 241–266.

Taylor, A. (1961). "X-ray Metallography". John Wiley & Sons, Inc., New York–London, 993 p.

Vishnyakov, Ya., Babareko, A., Vladimirov, S. and Egiz, I. (1979). "Theory of Texture Formation in Metals and Alloys". Nauka, Moscow, 329 p (in Russian).

Wcislak, L. and Bunge, H.J. (1996). "Texture Analysis with a Position Sensitive Detector". Cuvillier Verlag, Göttingen, 213 p.

Wcislak, L., Bunge, H.J. and Nauer-Gerhardt, C. (1993). X-ray diffraction texture analysis with a position sensitive detector. *Z. Metallkunde*, **84**, 479–493.